Test of the FDTD accuracy in the analysis of the scattering resonances associated with high-*Q* whispering-gallery modes of a circular cylinder

Artem V. Boriskin,[1,*] Svetlana V. Boriskina,[2] Anthony Rolland,[3] Ronan Sauleau,[3] and Alexander I. Nosich[1]

[1]*Institute of Radiophysics and Electronics NASU, Kharkiv, Ukraine*
[2]*Department of Electrical and Computer Engineering, Boston University, Boston, Massachusetts, USA*
[3]*Institut d'Electronique et de Télécommunications de Rennes, Université de Rennes 1, Rennes cedex, France*
**Corresponding author: a_boriskin@yahoo.com*

Received February 4, 2008; accepted March 13, 2008;
posted March 26, 2008 (Doc. ID 92470); published April 28, 2008

Our objective is the assessment of the accuracy of a conventional finite-difference time-domain (FDTD) code in the computation of the near- and far-field scattering characteristics of a circular dielectric cylinder. We excite the cylinder with an electric or magnetic line current and demonstrate the failure of the two-dimensional FDTD algorithm to accurately characterize the emission rate and the field patterns near high-*Q* whispering-gallery-mode resonances. This is proven by comparison with the exact series solutions. The computational errors in the emission rate are then studied at the resonances still detectable with FDTD, i.e., having *Q*-factors up to 10^3. © 2008 Optical Society of America

OCIS codes: 000.4430, 000.3860, 220.0220, 230.5750, 290.0290.

1. INTRODUCTION

Spherical, toroidal, circular-cylindrical, and some other open dielectric resonators are known to support so-called whispering-gallery-mode (WGM) natural oscillations [1,2]. The famous features of WGMs are tight confinement of their inner field near the resonator boundary and "exponentially high" radiation *Q*-factors. Circular-disk dielectric resonators are the key components in many advanced optical circuits including filters, couplers, laser cavities, etc. [1–3]. This is due to their ability to support the WGM-like natural oscillations provided that the disk thickness is not too small and the radius is much larger than the wavelength. Among new configurations not mentioned in [1,2], there are thin disks embedded into a photonic-crystal matrix [4], coupled into a cyclic photonic molecule [5], and built into a coupled-resonator optical waveguide [6]. These coupled microresonators may provide additional advantages such as further lowering of the thresholds of lasing [7,8], improvement of emission directionality [4], and low-loss bending [9].

The available lithographic, epitaxial, and etching technologies enable controlled fabrication of thin microdisk resonators of a given size and thickness. Still, due to fine nature of the WGM effects exploited in the optical and photonic devices, their accurate preliminary modeling may provide great savings in the cost and time of design.

Among the available numerical techniques used in computational photonics is the finite-difference time-domain (FDTD) method [10,11]. Although FDTD is well known as a powerful and flexible tool, it has drawbacks also widely discussed in literature, namely, the numerical dispersion, staircase boundary approximation, and back-reflection from the borders of the computational window. These drawbacks become critical if physical boundaries of the studied object do not coincide with the mesh and/or if high-*Q* resonances are involved [12–14]. Both problems are present if a WGM resonator is considered.

It is known that a thin microdisk resonator can be studied in 2D formulation with its bulk refractive index replaced by the effective index provided that the radius is considerably larger than the thickness and the wavelength [15]. This is because the effective index is taken as the normalized propagation constant of one of the guided modes on the infinite dielectric slab of the same thickness and bulk refractive index [16]. Therefore accurate 2D modeling of WGMs is an important task in computational photonics. Reduction of dimensionality significantly reduces the time and memory consumption for FDTD algorithms, and thus enables one to choose denser meshes and smaller time steps. This may improve the accuracy of simulations within reasonable timing [17,18]. Additionally, various techniques have been proposed to improve the performance of FDTD solvers (see, e.g., [10,19] and references therein). As a result, reasonable agreement between the FDTD and the experiment is often reported [18]. Assessment of the FDTD algorithms accuracy performed by comparison with numerical algorithms based on different techniques is also available in literature, e.g., [12,14]. Nevertheless, the domain of trusted applicability for the FDTD solutions is still not completely clear because in most cases they have been compared with other approximate solutions to the Maxwell equations that have no built-in criteria of accuracy. Exception is the paper [12], where FDTD and method-of-moments (MoM) re-

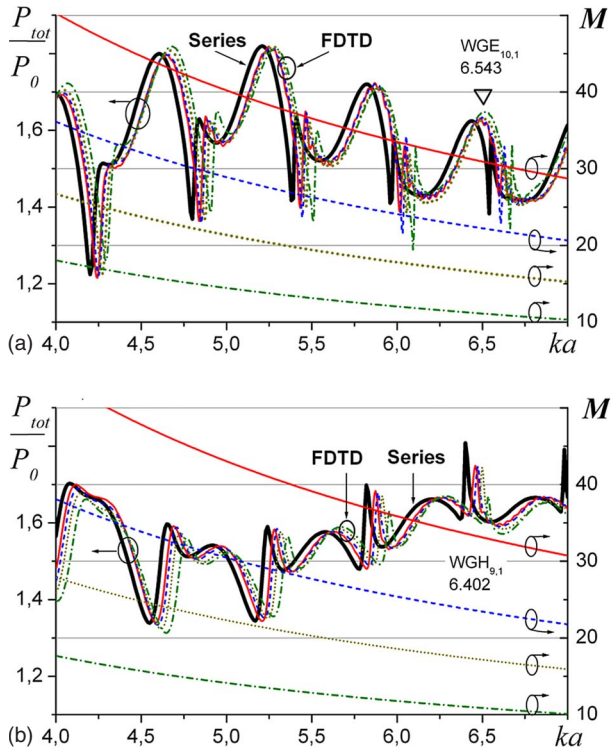

Fig. 1. (Color online) Normalized total emission rate of the line source illuminating quartz ($\sqrt{\varepsilon}=2.0$) circular resonator computed by the FDTD method and Series (thick solid curves): (a) E-polarization and (b) H-polarization. The family of four FDTD curves is computed with different meshes. The values of M for each FDTD curve are represented by the monotonic lines of corresponding types.

sults were compared with Mie-type series data for the backward scattering cross-sections of the magnetodielectric hollow circular cylinder illuminated by the normally incident plane electromagnetic wave. Conclusions of [12] were far from optimistic: in fact, both MoM and FDTD showed 100% and larger errors in the vicinity of sharp resonances that were associated with the modes that were still not truly WGM ones.

2. OUTLINE OF THE SOLUTION

To shed further light on this issue and specifically target WGMs, we study numerically the near- and far-field characteristics of a single dielectric circular cylinder illuminated by a parallel line source (point source in 2D). We compare the results computed by the conventional FDTD code and by the analytical series solution. This enables us to assess the accuracy of conventional FDTD code in the vicinities of high-Q WGM resonances. We also compute the complex-valued natural frequencies of the WGMs to estimate the associated radiation Q-factors. This is done by means of an iterative gradient-type algorithm applied to the rigorous characteristic equation,

$$J_m(ka\sqrt{\varepsilon})H_m'(ka) - \sqrt{\varepsilon}H_m(ka)J_m'(ka\sqrt{\varepsilon}) = 0, \qquad (1)$$

where $J_m(\cdot)$ and $H_m(\cdot)$ are the Bessel and Hankel functions, $m=0,1,\ldots$, the prime denotes the differentiation in argument, k is the free-space wavenumber, a is the cylinder radius, and ε is its dielectric constant.

Our in-house 2D FDTD algorithm has been developed based on the standard method proposed by Yee [20]. The Cartesian mesh has been used for the computational space surrounded with the perfectly matched layers (PML) [21]. As a primary source, we use a line current modulated in time with a Gaussian pulse and set the parameters of PML that provide the normal backreflection from the layer boundary below −50 dB for the entire considered frequency range. The time is discretized in accordance to the Courant stability criterion. (*) see comment below

As reference data, we take the analytical solution built by using the separation of variables. This solution has the form of infinite series whose coefficients depend on the cylindrical functions. As they can be computed with machine precision, the accuracy of the series algorithm is controlled by the truncation order, N, provided that it exceeds $ka\sqrt{\varepsilon}$. We keep $N=ka\sqrt{\varepsilon}+20$; thus the accuracy is at least 10^{-8}.

3. NUMERICAL RESULTS

First, we consider a circular dielectric cylinder made of quartz ($\sqrt{\varepsilon}=2.0$) excited by an electric or magnetic line current located at the distance equal to the resonator radius, a, from its boundary. Figure 1 presents the total power radiated by the line source in the presence of a cylinder normalized by the same value for a stand-alone line source,

$$P_0 = 2/Z_0k \quad (\text{E-pol.}), \quad P_0 = 2Z_0/k \quad (H\text{-pol.}), \qquad (2)$$

versus the normalized frequency (Z_0 is the free-space impedance). This quantity is the same as the normalized spontaneous emission rate in the source plus cavity system. In the analytical solution, it is reduced to the series with known coefficients. In the FDTD case, we computed the transient field values on auxiliary contour between the cylinder and the boundary of the computational window and then integrated them into the total radiated power.

Results obtained with the FDTD and series algorithms relate to the left-side scale in Fig. 1, and the FDTD mesh size parameter, M, relates to the right-side scale. The thick solid line represents the reference series solution, while the family of four thin curves of different types is obtained by the FDTD algorithm with different mesh sizes taken as λ_e/M, where λ_e is the wavelength in material. With a transient excitation, the FDTD method pro-

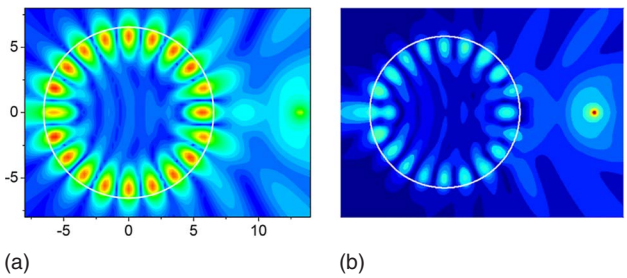

Fig. 2. (Color online) Normalized near-field maps of quartz circular resonators excited by the E-polarized line source: (a) Series ($ka=6.543$) and (b) FDTD ($ka=6.600$). The corresponding WGM-$E_{10,1}$ resonance is indicated by the triangle in Fig. 1(a).

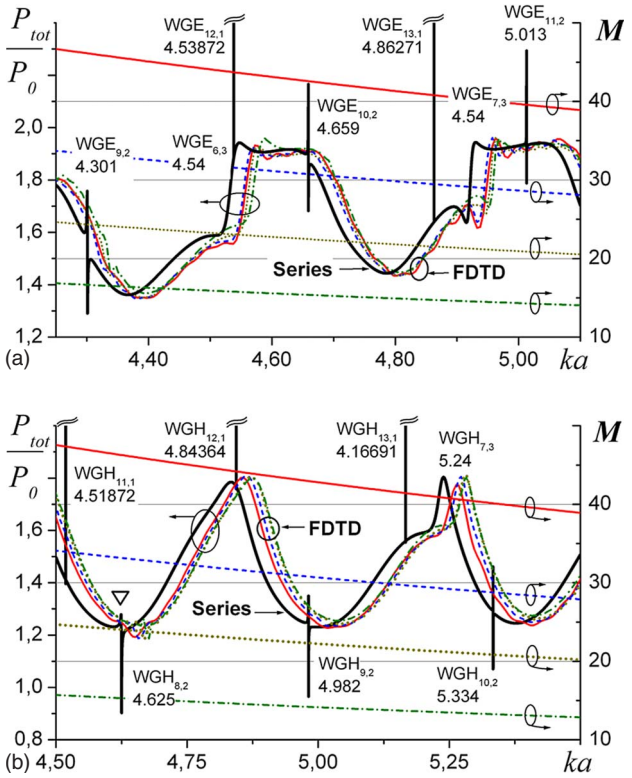

Fig. 3. (Color online) Same as in Fig. 1 but for a silicon resonator ($\sqrt{\varepsilon}=3.42$).

vides results over a wide frequency range in a single calculation. Although this is a great benefit compared to the frequency domain methods, the accuracy of results differs within that range. It depends on the varying mesh size, which is indicated by four monotonically lowering curves of the corresponding types.

Periodic spikes, well seen in Fig. 1, correspond to the WGM-type $E_{m,1}$ and $H_{m,1}$ resonances. This is confirmed by their periodicity and the characteristic in-resonance near-field patterns presented in Fig. 2 for the E-case. In this notation, the indices indicate the number of the field function variations along the azimuth and the radius, respectively. As known, the higher the resonant frequency (equivalently, the denser the material and the larger the m), the higher the radiation quality factor Q. For the WGM resonances in the lossless cylinder ($\mathrm{Im}\sqrt{\varepsilon}=0$), it behaves as $Q\sim\exp(\sqrt{\varepsilon}\,\mathrm{Re}\,ka)$, while for non-WGM ones it behaves as $Q\sim\sqrt{\varepsilon}\,\mathrm{Re}\,ka$.

Comparison of the curves obtained by two methods shows that the FDTD algorithm displays a regular shift of the whole curve to the higher frequencies. This can be explained by the staircase approximation of the cylinder boundary that is intrinsic for all conventional FDTD algorithms, so that actual domain filled in with dielectric is slightly smaller that the circle of radius a. Because of this shift, the FDTD algorithm becomes especially inaccurate near the resonance frequencies. The shift can be reduced to a certain value by choosing a denser mesh. However, it cannot be eliminated completely and the minimum accessible error is apparently determined by the backreflections from the virtual boundary of the computational window; thus, it depends on the type of the nonreflecting boundary condition used and the shape and size of the computational window. This conclusion is in line with the earlier studies, e.g., see [12,22].

The curves in Fig. 3 are similar to Fig. 1 but computed for the line-source excited cylinder made of silicon ($\sqrt{\varepsilon}=3.42$). Here, the radiation Q-factors of WGM-type natural modes are larger, and accurate characterization of corresponding resonance spikes in the spontaneous emission rate with FDTD becomes troublesome. Note that for a silicon resonator higher-radial-order WGMs are also excited. Those detectable in Fig. 3 are of the first to the third order radial modes that are confirmed by the in-resonance near-field patterns presented in Fig. 4. Although the FDTD patterns in Figs. 2(b) and 4(b) have been computed at the corresponding (shifted) frequencies and with a dense mesh ($M=50$), they are still quite inaccurate compared to the exact ones computed by the series algorithm (Figs. 2(a) and 4(a), respectively).

This reveals that, in principle, the spikes associated with higher-Q resonances experience more difficulties when computed with FDTD algorithms. Therefore it is quite important to have *a priori* information about the quality factors of natural modes, which can be involved in the solution of the considered problem in order to foresee the errors potentially entering the numerical solution. In general, this can only be done by solving the corresponding eigenvalue problem that may be difficult, especially for arbitrarily shaped resonators.

Here, note that FDTD algorithms are not able to solve the eigenvalue problems in a direct manner; this has been emphasized in [3] in relation to the lasing modes. Instead, the FDTD method always needs a pulsing source placed at some point inside or near a cavity and operates with the output in the form of the time-domain signal computed at some other point (see, e.g., [23]). Further the Q-factors of detected natural modes are extracted from that signal by using Fourier transform. Therefore the result depends on the good or bad choice of the source and observation points and on the accuracy of numerically performed Fourier transform, to mention only the obvious factors. Such an approach suffers from too many errors and may give only a rough estimation of the associated Q-factors; however, it still finds wide use in optical simulations.

(*) see comment below

The scattering analysis seems to be less subject to such errors. However, as we will see below the matter is worse

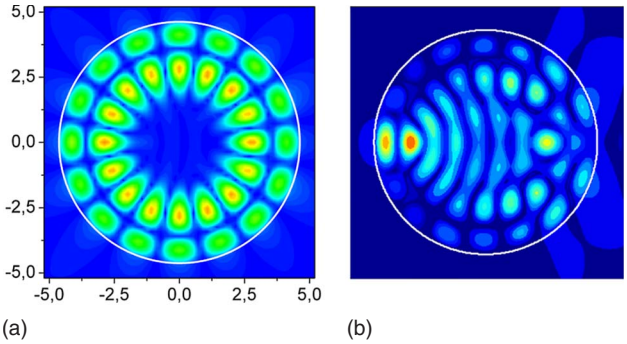

Fig. 4. (Color online) Normalized near-field maps of the silicon circular resonators excited by a line H-polarized current: (a) Series ($ka=4.625$) and (b) FDTD ($ka=4.645$). The corresponding WGM-$H_{8,2}$ resonance is indicated by the triangle in Fig. 3(b).

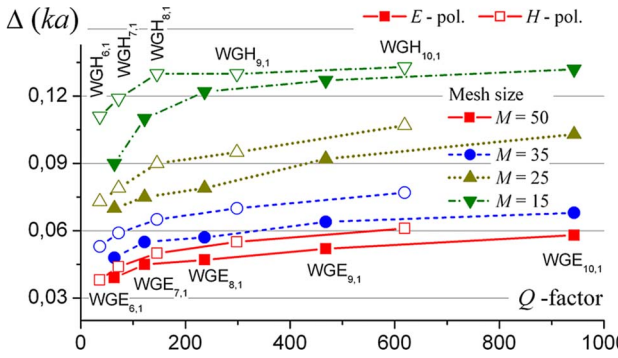

Fig. 5. (Color online) Normalized frequency shift extracted from comparison between FTDT and Series solutions for the WGM-related spikes in the normalized emission rate observed in Fig. 1 for the quartz resonator versus the resonances Q-factor. The family of four curves is for different mesh sizes.

than it is normally assumed; FDTD apparently fails to detect the contribution of natural-mode spikes that have Q-factors larger than some threshold values.

In Figs. 5 and 6, we present the behavior of the FDTD computational errors in the frequency locations and in the absolute values, respectively, of the spikes of the normalized spontaneous emission rate corresponding to the WGM resonances visible in Fig. 1, i.e., for the quartz cylinder. They are presented as (discrete-valued) functions of the Q-factors of associated natural modes obtained by solving Eq. (1). One can see that as soon as the radiation Q-factor exceeds 10^2, both errors start growing proportionally to the Q-factors.

Further, we have tried to extend the analysis of the FDTD errors to the resonances on the WGMs with higher Q-factors. As an example, exact radiation Q-factors of the modes having two field variations in radius, i.e., WGM-$E_{m,2}$ and WGM-$H_{m,2}$ with $m=8-11$ are presented for the silicon cylinder in Table 1. We have found, however, that our FDTD algorithm is not capable of detecting the resonances on the WGMs with Q-factors higher than 10^3. Therefore the higher-Q resonances, for instance, those on the WGM-$E_{m,1}$ and WGM-$H_{m,1}$ modes that are observed in Fig. 3 on the curves computed via the series, are missing on all the FDTD curves.

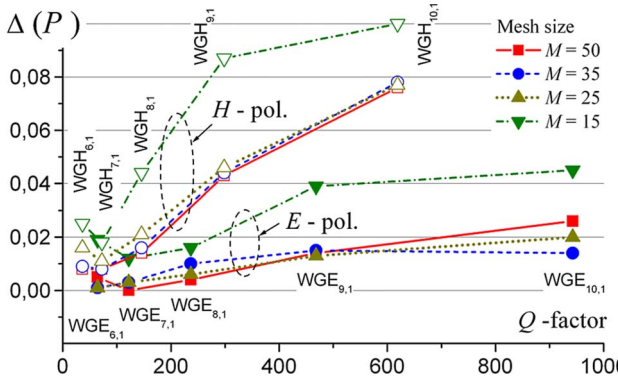

Fig. 6. (Color online) Computation errors of the FDTD algorithm for the normalized emission rate extracted from comparison between FTDT and Series solutions presented in Fig. 1 for the quartz resonator versus the resonances Q-factor. The family of four curves is for different mesh sizes.

Table 1. Q-Factors of the (m,2) WGMs in a Silicon Circular Resonator

WGM-$E_{m,2}$			WGM-$H_{m,2}$		
m	ka	Q	m	ka	Q
9	4.30093	7862.90	8	4.62489	7380.38
10	4.65906	30,946.36	9	4.98161	31,393.24
11	5.01269	127,414.73	10	5.33371	137,516.08

Note that radiation Q-factor values of the same range, i.e., several thousand, are characteristic not only of the WGM oscillations in the uniform circular or spherical cavities of moderate optical size but also of the WGMs in nonuniform discrete Luneburg lenses [24] and printed antennas on spherical substrates [25], bow-tie modes in the stadium cavities [26], half-bow-tie modes in the extended hemielliptic lenses [27,28], and many other important configurations. Therefore corresponding resonances in their scattering characteristics are not accessible with conventional FDTD codes and need finer simulation tools.

(*) see comment below

4. CONCLUSION

The accuracy of the FDTD algorithm as to the characterization of high-Q WGM resonances in the emission rate of a line source near a circular cylindrical resonator has been tested against the exact series solution. Comparison of numerical results confirmed reasonable accuracy of FDTD when applied out of high-Q WGM resonances, as well as a rapid growth of the computational error near such resonances. Denser meshing reduces these errors to the level determined apparently by the type of absorbing boundary conditions used, shape and size of computational window, and other details of the FDTD code, but does not eliminate them. The growth of the errors proportionally to the natural-mode Q-factors has been demonstrated. Finally, a complete failure of conventional FDTD code in the detection of WGM resonances with radiation Q-factors significantly higher than 10^3 has been observed.

(*) see comment below

REFERENCES

1. A. B. Matsko and V. S. Ilchenko, "Optical resonators with whispering-gallery modes—Part I: basics," IEEE J. Sel. Top. Quantum Electron. **12**, 3–14 (2006).
2. V. S. Ilchenko and A. B. Matsko, "Optical resonators with whispering-gallery modes—Part II: applications," IEEE J. Sel. Top. Quantum Electron. **12**, 15–32 (2006).
3. A. I. Nosich, E. I. Smotrova, S. V. Boriskina, T. M. Benson, and P. Sewell, "Trends in microdisk laser research and linear optical modelling," Opt. Quantum Electron. (to be published); available at http://www.springerlink.com/content/x74382234u02608v/.
4. S. V. Boriskina, T. M. Benson, P. Sewell, and A. I. Nosich, "Directional emission, increased free spectral range, and mode Q-factors of 2-D wavelength-scale optical microcavity structures," IEEE J. Sel. Top. Quantum Electron. **12**, 1175–1182 (2006).
5. P. W. Evans and N. Holonyak Jr., "Room temperature photopump laser operation of native-oxide-defined coupled GaAs-AlAs superlattice microrings," Appl. Phys. Lett. **69**, 2391–2393 (1996).

6. A. Yariv, Y. Xu, R. K. Lee, and A. Scherer, "Coupled-resonator optical waveguide: a proposal and analysis," Opt. Lett. **24**, 711–713 (1999).
7. E. I. Smotrova, A. I. Nosich, T. M. Benson, and P. Sewell, "Threshold reduction in a cyclic photonic molecule laser composed of identical microdisks with whispering-gallery modes," Opt. Lett. **31**, 921–923 (2006).
8. P.-T. Lee, T.-W. Lu, J.-H. Fan, and F.-M. Tsai, "High quality factor microcavity lasers realized by circular photonic crystal with isotropic photonic band gap effect," Appl. Phys. Lett. **90**, 151125 (2007).
9. S. V. Pishko, P. D. Sewell, T. M. Benson, and S. V. Boriskina, "Efficient analysis and design of low-loss WGM coupled resonator optical waveguide bends," J. Lightwave Technol. **25**, 2487–2494 (2007).
10. K. L. Shlager and J. B. Schneider, "A selective survey of the finite-difference time-domain literature," IEEE Antennas Propag. Mag. **37**, 39–57 (1995).
11. A. Taflove and S. C. Hagness, *Computational Electrodynamics: The Finite-Difference Time-Domain Method*, 3rd ed. (Artech House, 2005).
12. G. L. Hower, R. G. Olsen, J. D. Earls, and J. B. Schneider, "Inaccuracies in numerical calculations of scattering near natural frequencies of penetrable objects," IEEE Trans. Antennas Propag. **41**, 982–986 (1993).
13. K. Phan-Huy, A. Morand, D. Amans, and P. Benech, "Analytical study of the whispering-gallery modes in two-dimensional microgear cavity using coupled-mode theory," J. Opt. Soc. Am. B **22**, 1793–1804 (2005).
14. Y. Liu, C. D. Sarrisa, and G. V. Eleftheriades, "Triangular-mesh-based FDTD analysis of 2-D plasmonic structures supporting backward waves at optical frequencies," J. Lightwave Technol. **25**, 938–946 (2007).
15. E. I. Smotrova, A. I. Nosich, T. Benson, and P. Sewell, "Cold-cavity thresholds of microdisks with uniform and non-uniform gain: quasi-3D modeling with accurate 2D analysis," IEEE J. Sel. Top. Quantum Electron. **11**, 1135–1142 (2005).
16. D. Marcuse, *Light Transmission Optics*, Computer Science and Engineering Series (Van Nostrand Reinhold Electrical, 1989).
17. S. C. Hagness, D. Rafizadeh, S. T. Ho, and A. Taflove, "FDTD microcavity simulations: design and experimental realization of waveguide-coupled single-mode ring and whispering-gallery-mode disk resonators," J. Lightwave Technol. **15**, 2154–2165 (1997).
18. A. Sakai and T. Baba, "FDTD simulation of photonic devices and circuits based on circular and fan-shaped microdisks," J. Lightwave Technol. **17**, 1493–1499 (1999).
19. Y. Liu and C. D. Sarris, "Fast time-domain simulation of optical waveguide structures with a multilevel dynamically adaptive mesh refinement FDTD approach," J. Lightwave Technol. **24**, 3235–3248 (2006).
20. K. S. Yee, "Numerical solution of initial boundary value problems involving Maxwell's equations in isotropic media," IEEE Trans. Antennas Propag. **14**, 302–307 (1966).
21. L.-P. Berenger, "Perfectly matched layer for the FDTD solution of wave-structure interaction problem," IEEE Trans. Antennas Propag. **44**, 110–118 (1996).
22. A. V. Boriskin, A. Rolland, R. Sauleau, and A. I. Nosich, "Assessment of FDTD accuracy in the compact hemielliptic dielectric lens antenna analysis," IEEE Trans. Antennas Propag. **56**, 758–764 (2008).
23. Y.-Z. Huang, Q.-Y. Lu, W.-H. Guo, and L.-J. Yu, "Analysis of mode characteristics for equilateral triangle semiconductor microlasers with imperfect boundaries," IEE Proc.: Optoelectron. **151**, 202–204 (2004).
24. A. V. Boriskin and A. I. Nosich, "Whispering-gallery and Luneburg lens effects in a beam-fed circularly-layered dielectric cylinder," IEEE Trans. Antennas Propag. **50**, 1245–1249 (2002).
25. S. Rondineau, A. I. Nosich, J.-P. Daniel, M. Himdi, and S. S. Vinogradov, "MAR-based analysis of a spherical-circular printed antenna with a finite ground excited by an axially-symmetric probe," IEEE Trans. Antennas Propag. **52**, 1270–1280 (2004).
26. S.-Y. Lee, M. S. Kurdoglyan, S. Rim, and C.-M. Kim, "Resonance patterns in a stadium-shaped microcavity," Phys. Rev. A **70**, 023809 (2004).
27. A. V. Boriskin, A. I. Nosich, S. V. Boriskina, T. M. Benson, P. Sewell, and A. Altintas, "Lens or resonator?—Electromagnetic behavior of an extended hemielliptic lens for a sub-mm wave receiver," Microwave Opt. Technol. Lett. **43**, 515–518 (2004).
28. A. V. Boriskin, G. Godi, R. Sauleau, and A. I. Nosich, "Small hemielliptic dielectric lens antenna analysis in 2-D: boundary integral equations versus geometrical and physical optics," IEEE Trans. Antennas Propag. **56**, 485–492 (2008).

(*) Later it has been revealed that the source of the reported errors in the shape and location of sharp WGM resonances and the failure of detection, with in-house FDTD code, of the resonances having Q-factors larger than 10^4 is in not sufficiently large integration interval in the numerical Fourier transformation of the time-domain signal to the frequency spectrum.